Modelling Instantaneous Firing Rate of DBS Target Neuronal Ensembles in Basal Ganglia and Thalamus

running title: Firing Rate Model on Neurons Receiving DBS

Yupeng Tian, MS[1,2,4,5]; Matthew J. H. Murphy, BS[6]; Leon A Steiner, PhD[1,7,8]; Suneil K Kalia, PhD[1,4,5,8,10]; Mojgan Hodaie, PhD[1,5,8,10]; Andres M Lozano, PhD[1,5,8,10]; William D Hutchison, PhD[3,5,8]; Milos R. Popovic, PhD[2,4,5]; Luka Milosevic, PhD[1,2,4,5]; Milad Lankarany, PhD[1,2,3,4,5]**

[1] Krembil Research Institute – University Health Network, Toronto, ON, Canada

[2] Institute of Biomedical Engineering, University of Toronto, Toronto, ON, Canada

[3] Department of Physiology, University of Toronto, Toronto, ON, Canada

[4] KITE Research Institute, Toronto Rehabilitation Institute - University Health Network, Toronto, ON, Canada

[5] CRANIA, University Health Network and University of Toronto, Toronto, Canada.

[6] Department of Mathematics, University of Toronto, Toronto, ON, Canada

[7] Berlin Institute of Health (BIH), Germany

[8] Department of Surgery, University of Toronto, Toronto, Canada

[9] Department of Neurology, Charité-Universitätsmedizin Berlin, Germany

[10] Division of Neurosurgery, Toronto Western Hospital, University Health Network, Toronto, Canada

Funding

This project was supported by Milad Lankarany's NSERC Discovery Grant (RGPIN-2020-05868). Leon A Steiner received grant support from Deutsche Forschungsgemeinschaft (DFG, German Research Fundation) – Project-ID 424778381 – TRR 295. Leon A Steiner received additional funding through the Junior Clinician Scientist Program of the Berlin Institute of Health and though a postdoc scholarship provided by the German Academic Exchange Service - DAAD.

Author Contributions

Yupeng Tian and Milad Lankarany were responsible for the conception and design of the work. Leon A Steiner, Suneil K Kalia, Mojgan Hodaie, Andres M Lozano, William D Hutchison and Luka Milosevic were responsible for the acquisition of data. Yupeng Tian and Matthew J. H. Murphy were responsible for analyzing the data. Yupeng Tian, Milos R. Popovic, and Milad Lankarany were responsible for interpreting the data. Yupeng Tian and Milad Lankarany were responsible for drafting the work. All authors are responsible for revising the work critically for important intellectual content. All authors approved the final version of the manuscript, and agree to be accountable for all aspects of the work in ensuring that questions related to the accuracy or integrity of any part of the work are appropriately investigated and resolved. All persons designated as authors qualify for authorship, and all those who qualify for authorship are listed.

Conflict of Interest

All authors declare no conflict of interest.

**** To whom correspondence should be addressed:***

Milad Lankarany

The Krembil Research Institute – University Health Network (UHN)

60 Leonard Ave, Toronto, M5T 0S8, Canada

Telephone: 416-602-4391

Email: Milad.Lankarany@uhnresearch.ca

ABSTRACT

Objective: Parkinson's disease (PD) is the second most common neurodegenerative disorder symptom, and is closely related to the dysfunction of the basal ganglia-thalamocortical network. Deep Brain Stimulation (DBS) is an effective treatment for suppressing PD motor symptoms; however, the underlying mechanisms of DBS remain elusive. A recent study demonstrated that different nuclei of the basal ganglia and thalamus respond differently to various frequencies of DBS. Despite the capability of existing models in interpreting experimental data qualitatively, there are very few unified computational models that quantitatively capture the dynamics of the neuronal activity of varying stimulated nuclei—including subthalamic nucleus (STN), substantia nigra pars reticulate (SNr) and ventralis intermedius (Vim)—across different DBS frequencies.

Materials and Methods: Both synthetic and experimental data were utilized in model fits; the synthetic data were the simulations from an established spiking neuron model, and the experimental data were the single-unit recordings during DBS (microstimulation). Based on these data, we developed a novel mathematical model to represent the firing rate of neurons receiving DBS, including neurons in STN, SNr and Vim—across different DBS frequencies. In our model, the DBS pulses are filtered through a synapse model and a nonlinear transfer function to formulate the firing rate variability. To consistently fit the model in varying frequencies of DBS, we developed a novel parameter optimization method based on the concatenated data from all DBS frequencies.

Results: Our model accurately reproduces the firing rates observed and calculated from both synthetic and experimental data. The optimal model parameters are consistent across different

DBS frequencies, and this consistency conforms to the relatively static synaptic structures in short durations of DBS.

Conclusion: Our model can detect the firing rate dynamics in response to DBS, and potentially implemented in navigating the DBS parameter space and improving DBS clinical effects.

Keywords: Deep Brain Stimulation, basal ganglia, thalamus, rate model, short-term synaptic plasticity

INTRODUCTION

Parkinson's disease (PD) is the second most common neurodegenerative disorder [1], and is characterized by motor symptoms like stooped posture, shuffling gait (festination), akinesia, rigidity, and rest tremor [2]. Development of these symptoms is thought to be mostly related to the pathological changes in the basal ganglia-thalamocortical network (BGTCN) [3]. Deep brain stimulation (DBS) has become a standard therapy for movement disorders, including PD [3], essential tremor [4], and dystonia [5]. DBS has also been investigated for therapeutic effects of psychiatric and cognitive disorders, including obsessive-compulsive disorder [6], Alzheimer's disease [7] and epilepsy [8]. Despite the established benefits of DBS, its therapeutic mechanism on neuronal activity is not yet well understood [9,10]. Moreover, efforts on optimizing DBS parameters (e.g., stimulation frequency, pulse width) to achieve the maximal clinical benefit have largely relied on trial-and-error strategies in which neurologists observe the immediate effects of DBS [9,11,12]. Boutet et al. [9] have recently developed a machine learning algorithm to infer the optimal DBS parameters based on the physiological consequences of the related brain circuits recorded

with functional magnetic resonance imaging (fMRI). However, the detailed physiological effects of the critical DBS parameters, e.g. the stimulation frequency, remained elusive. Synaptic depression, which can stem from synaptic and axonal failure [13], was suggested as the main biophysical explanation to the intermittent firing patterns of stimulated nuclei (specifically for STN) in high frequency DBS [14]. Recently, Milosevic et al. [10] demonstrated that different frequencies of DBS modulate the firing rate of the stimulated nuclei differently. During low frequency DBS, the ratio of excitatory and inhibitory pre-synaptic inputs influences the firing rate of stimulated neurons. In high frequency DBS, stimulated neurons are mostly suppressed due to synaptic depression [10]. Nevertheless, detailed quantified dynamics underpinning the experimental firing rate of the stimulated neurons in response to different DBS frequencies were left unknown. Additionally, there is no systematic or automatic method to optimize the model parameters across different DBS frequencies.

The firing rate of a population of neurons—which might be modulated by DBS—is a representative feature of the underlying neuronal dynamics, and has been widely used in the modeling of the sensory cortex [15,16], the visual cortex [17], Parkinson's Disease [18] and cultured network [19]. Despite the significance of firing rate, the existing models on DBS-induced neuronal dynamics are often based on the variability in the membrane potential, or oscillations observed in the local field potentials (LFP) [10,11,20]. The spiking neuron models aim to replicate the neuronal dynamics of single neurons [10,13], while abstract models were developed to track neuronal activities recorded by macro electrodes, e.g., LFP [11,21]. Milosevic et al. [10] utilized a model for short-term synaptic plasticity, together with a leaky integrate-and-fire (LIF) model, to track firing patterns of stimulated nuclei qualitatively. Yousif et al. [11,21] developed macroscopic Wilson-Cowan [22] mean-field models on the neuronal network underlying neurological movement disorders, including PD

and essential tremor (ET); they implemented the models to approximate the pathological LFP oscillations, including the tremor-range oscillations of ET and the Parkinsonian beta band oscillations. Despite the recognized benefits of these models, they cannot track changes in the *instantaneous firing rate* quantitatively; in particular, these models cannot capture the dynamics of the firing rate of the stimulated nuclei across various DBS frequencies. In this work, we developed a firing rate model to reproduce the instantaneous firing rate of stimulated neurons during various frequencies of DBS.

The developed rate model was utilized to mimic instantaneous firing rates of neurons receiving DBS in three basal ganglia and thalamic nuclei, namely, STN, SNr and Vim. We explored the firing rate dynamics in response to different ratios of excitatory and inhibitory presynaptic inputs, during various frequencies of DBS (5 to 200Hz). Importantly, we incorporated the dynamics of short-term synaptic plasticity (STP) [23] in modeling the presynaptic inputs. STP reflects immediately reversible effects of the synapses upon the removal of external stimuli [10], and is essentially important in various brain functions, e.g., motor control [10], speech recognition [23] and working memory [24]. The integration of STP in the computational modelling can greatly enrich the model's information processing capability and neuronal behavior predictability [23]. Moreover, we developed a robust optimization method based on the concatenated signal across different DBS frequencies. For fitting our rate model to DBS data, our "concatenated-frequencies" optimization method is different from the commonly used methods that consider only a single DBS frequency [21], or adjust the model parameters manually [11,14]. With our concatenated-frequencies optimization method, we obtained a single set of optimal model parameters—which is consistent across varying DBS frequencies—for each targeted nuclei. Such consistency in model parameters conforms to the short duration of our DBS recordings ($\leq$ 10s for all DBS frequencies) on each nuclei; the

synaptic anatomical structure mostly remains static in response to short (seconds to minutes) external stimuli [25]. Furthermore, our concatenated-frequencies optimization method is significantly more accurate than the method incorporating only a single DBS frequency (see **Results**). Our developed rate model and the parameter optimization method could accurately reproduce the instantaneous firing rates of various basal ganglia and thalamic neurons receiving different frequencies of DBS. Our model fits well for both synthetic and experimental DBS data. Our work can provide a framework to study the instantaneous effects of DBS parameters on neuronal activity, and may help navigating the DBS parameter space and improve DBS clinical effects.

MATERIALS AND METHODS

We implemented the same experimental single-unit recordings as published in Milosevic et al. [10]. Thus, the commitment to ethics policies have already been validated [10]. All experiments conformed to the guidelines set by the Tri-Council Policy on Ethical Conduct for Research Involving Humans and were approved by the University Health Network Research Ethics Board [10]. Moreover, each patient provided written informed consent prior to taking part in the studies [10].

Method Overview

We developed a rate model to describe the instantaneous firing rate of a population of local neurons receiving DBS. We utilized a sigmoid function to transfer the impact of DBS-induced short-term synaptic plasticity [10] to the variability of the firing rate that is expressed by a first order ordinary differential equation (ODE). Specifically, DBS pulses were filtered by the Tsodyks &

Markram (TM) model of short-term synaptic plasticity [26], and fed to the firing rate differential equation through a sigmoid nonlinear function. In order to estimate the parameters for the nonlinear function and the differential equation, we constructed peristimulus time histograms (PSTH) of recorded spikes (for both synthetic and experimental data) as a reference for modeling instantaneous firing rates. The synthetic data are the simulations from the LIF model in Milosevic et al. [10] (see **Supplementary Method A**), and the experimental data are the single-unit recordings from 4 basal ganglia and thalamic nuclei—STN, SNr, Vim and Rt—across specific sets of DBS frequencies in 5~200Hz. Unlike the limitation in experimental data, we can simulate the synthetic data with arbitrary DBS frequencies. Thus, the purpose of fitting our rate model to the synthetic data is to validate the model generalizability, and to fully compare with other modeling methods. The model fits to synthetic and experimental data are also compared to investigate the improvements of the experimental data fit.

In both synthetic and experimental data, we inferred the optimal model parameters for each nuclei by concatenating spikes across different DBS frequencies. Using such concatenated-frequencies optimization method [27,28], we obtained the optimal rate model parameters by minimizing the sum of squared error (SSE) between the model output and the reference PSTH across all DBS frequencies.

The Synthetic Data

The synthetic data is the firing rate computed with PSTH on 20 spike trains simulated from the LIF model (see **Supplementary Method A**). By superimposing these spike trains from the LIF neurons, we compute the PSTH firing rate (P(t)) as follows:

$$P(t) = \frac{1}{ML}\sum_{i=1}^{M} n_{i,t} \quad (1)$$

where M is the number of neurons, L (ms) is the length of the PSTH kernel, $n_{i,t}$ is the number of spikes generated by the ith neuron in the PSTH kernel at time t, i.e., the interval $[t - \frac{L}{2}ms, t + \frac{L}{2}ms]$. The PSTH firing rate is updated with a time resolution dt = 0.1ms. The appropriate PSTH kernel length L should depend on individual data [29,30]. We use L = 20ms for data from Vim, Rt, and SNr; L = 50ms is used for data from STN.

We simulate LIF neurons with different DBS frequencies, including {5, 10, 20, 30, 50, 100, and 200Hz}. For each DBS frequency of each BGTCN nuclei, the simulation time is 1,000ms, with time step of dt = 0.1ms; the simulation stops at 1,000ms because the firing rate always reaches the steady state before 500ms. The maximal DBS frequency considered in this work for Vim, Rt, STN, and SNr are 200Hz, 200Hz, 100Hz, and 50Hz, respectively. Experimental data has demonstrated that the firing rate of STN and SNr for DBS frequencies (using 100μA and symmetric 0.3ms biphasic pulses) larger than these max frequencies is close to zero [10].

The Experimental Data

The experimental single-unit recordings and data protocols are from Milosevic et al. [10]. Microelectrodes were used to deliver DBS and record data, using 100μA and symmetric 0.3ms biphasic pulses (150us cathodal followed by 150us anodal) [10]. The recordings in STN, SNr and Rt were from patients with Parkinson's disease, and Vim recordings were obtained from patients with essential tremor [10]. For Vim and Rt, we recorded {5, 10, 20, 30, 50, 100, and 200Hz} DBS data of length {10, 5, 3, 2, 1, 5, and 2s}, respectively. The recording length of the 5Hz DBS data was 5 seconds for STN, and 10 seconds for SNr; we recorded {10, 20, 30, and 50Hz} DBS data of length {5, 3, 2, and 1s} for both STN and SNr. The recording length of the 100Hz DBS data for STN is 3 seconds.

For each DBS frequency on each nuclei, we recorded 5 to 8 spike trains from different patients. The time stamps of the DBS pulses have small deviations (~2%) because of the imperfect internal clock of the stimulator [31]; in the MATLAB script, we adjust the time stamps so that the DBS pulses are delivered with the accurate frequencies. Using the PSTH formulated in (1), we computed the reference firing rate from these spike trains. Thus, the PSTH firing rate is essentially the average firing rate across spike trains recorded from different patients, and we observed that the data from different individual patients are consistent [10].

DBS-induced Input into the Rate Model

The input to our rate model is the DBS-induced post-synaptic current (I_{syn}), and we formulate I_{syn} with the Tsodyks & Markram (TM) model on short-term synaptic plasticity (STP) [26]. Our formulation of the DBS input is more physiological than the common approach that model DBS effects as rectangular pulses [32,11,21].

For the neurons receiving DBS, we assume that each neuron receives inputs from 500 synapses [10], and the ratio of the number of excitatory synapses to inhibitory synapses is different for varying BGTCN nuclei, and is shown in **Supplementary Table 1**. The excitatory-inhibitory synaptic ratio has high variability in STN neurons [10,33]. The synaptic inputs to a minority of STN neurons are dominantly excitatory, whereas to a majority of STN neurons are dominantly inhibitory [33]. In this work, we analyze data recorded from STN neurons receiving evident inhibitory inputs (inhibitory synapses occupies 70%).

Each DBS pulse activates all pre-synaptic inputs simultaneously, and generates DBS-evoked spikes on the presynaptic terminals. The DBS-evoked spikes are filtered by the TM model,

generating the post-synaptic current, I_{syn}, that is obtained by a linear combination of presynaptic excitatory (I_{exc}) and inhibitory (I_{inh}) currents as follows:

$$I_{syn}(t) = w_{exc}\, I_{exc}(t) - w_{inh} I_{inh}(t) \quad (2)$$

where w_{exc} and w_{inh} denote the synaptic weights of the modeled excitatory and inhibitory currents, respectively; w_{exc} and w_{inh} vary for different BGTCN nuclei [10]. The values for these weights are summarized in **Supplementary Table 2**.

I_{exc} (respectively, I_{inh}) is the total post-synaptic current from all excitatory (respectively, inhibitory) synapses. Each synapse (excitatory or inhibitory) is modeled by the TM model for short-term synaptic plasticity.

$$\frac{du}{dt} = -\frac{u}{\tau_F} + U(1-u^-)\delta\left(t - t_{sp}\right) \quad (3)$$

$$\frac{dr}{dt} = \frac{1-r}{\tau_D} - u^+ r^- \delta\left(t - t_{sp}\right) \quad (4)$$

$$\frac{dI}{dt} = -\frac{I}{\tau_s} + A u^+ r^- \delta(t - t_{sp}) \quad (5)$$

where u indicates the utilization probability, i.e., the probability of releasing neurotransmitters in synaptic cleft due to calcium ion flux in the presynaptic terminal. The variable r indicates the fraction of available resources after the neurotransmitter depletion caused by neuronal spikes. We denote as u^- and r^- the corresponding variables just before the arrival of the spike; similarly, u^+ and r^+ refer to the moment just after the spike. Upon the arrival of each presynaptic spike t_{sp}, u increases by $U(1-u^-)$. If there is no presynaptic activity, u exponentially decays to zero; this decay rate is the facilitation time constant, τ_F. As well, the vesicle depletion process—due to the release of neurotransmitters—was modeled by (4) where r denotes the fraction of resources that remains available after the neurotransmitter depletion. In contrast to the increase of u upon the arrival of each presynaptic spike, r drops and then recovers to its steady state value of 1 (this

recovery rate is given by the depression time constant τ_D). The competition between the depression (τ_D) and facilitation (τ_F) time constants determines the dynamics of the synapse. In the TM model, U, τ_F, and τ_D are three parameters that determine the types of the synapse, namely, facilitation, pseudo-linear, and depression. The values of the TM model parameters differ across excitatory and inhibitory synapses, and are summarized in **Supplementary Tables 3(A)** & **4(A)**. In (5), I and τ_s indicate the post-synaptic current and its time constant, respectively. For an excitatory (respectively, inhibitory) synapse, τ_s is denoted as τ_{exc} (respectively, τ_{inh}); these time constants are shown in **Supplementary Table 2**. The absolute response amplitude A = 1 for all situations.

We obtain I_{exc} (respectively, I_{inh}) by adding the post-synaptic currents from all excitatory (respectively, inhibitory) synapses. Each BGTCN nuclei has different proportions of excitatory and inhibitory synapses. Within excitatory (respectively, inhibitory) synapses, the ratio of the 3 types of synapses, namely, facilitation, pseudo-linear, and depression, are also different among BGTCN nuclei (**Supplementary Tables 3(B)** & **4(B)**).

The Rate Model and the Parameter Optimization Method

We used a sigmoid transfer function to link the post-synaptic current (I_{syn} as defined in (2)) to the rate model on the firing rate of the stimulated nuclei. The rate model underlying a neuronal ensemble receiving DBS is stated as follows:

$$\tau \frac{dr}{dt} = -(r - r_b) + F(I_{syn}), \quad \text{where } F(I_{syn}) = \frac{c}{1+\exp\left[-s*(I_{syn}-k)\right]} \tag{6}$$

where $r(t)$ is the neuronal firing rate at time t and τ is the membrane time constant. For the sigmoid transfer function $F(I_{syn})$, c is the scaling parameter, s is the shape parameter, and k is the shift parameter. r_b is the baseline firing rate of the modelled nuclei. We confine r_b in biological constraints, based on experimental and synthetic data from both human and mammalian recordings.

For Vim, $r_b \in [10, 50]$ Hz [10,34]; for Rt, $r_b \in [3, 40]$ Hz [18,10]; for SNr, $r_b \in [40, 120]$ Hz [18,10]; for STN, $r_b \in [5, 100]$ Hz [10,35]. The initial value of $r(t)$ (denoted as r_{ini}) is computed by simulating a 10s spike train from the LIF model in Milosevic et al. [10] with the DBS – OFF condition for the modelled nuclei. r_{ini} is computed as: "total number of spikes"/10s; r_{ini}(Vim) = 39.3Hz, r_{ini}(Rt) = 5.0Hz, r_{ini}(SNr) = 57.4Hz, and r_{ini}(STN) = 27.6Hz. The rate model fit results for Vim, STN and SNr are shown in **Results**; Rt-DBS is a less common choice in clinics to obtain therapeutic effects [10], and the corresponding fit result is shown in **Supplementary Figure 2**.

We then inferred the parameter set $\Phi = \{\tau, r_b, c, s, k\}$ by minimizing the sum of squared errors (SSE) between the model output, $r(t)$, and the reference firing rate, $P(t)$ (the PSTH firing rate defined in (1)). We fit the parameters separately for different basal ganglia and thalamus nuclei. For each nuclei, the optimal parameter set Φ_{opt} is the same across all DBS frequencies; such consistency in model parameters conforms to the relatively static synaptic anatomical structure in response to short (seconds to minutes) external stimuli [25] (in our case, $\leq$ 10s for all DBS data).

In the case of both experimental and synthetic data, for the fitting process in the simulation, the sampling resolution is dt = 0.1ms. We ran independent simulations for each DBS frequency and the simulated signal is denoted as $r_{fq}(\Phi, t) = \{ r_{fq}(\Phi, t_1), \dots , r_{fq}(\Phi, t_N)\}$, which corresponds to a certain DBS frequency (fq) and parameter set Φ; N is the total number of time points. Similarly, the reference PSTH is denoted as $P_{fq}(t) = \{ P_{fq}(t_1), \dots , P_{fq}(t_N)\}$. Given the rate model and reference PSTH, the SSE function is:

$$SSE_{fq}(\Phi) = \| \boldsymbol{r}_{fq}(\Phi, \boldsymbol{t}) - \boldsymbol{P}_{fq}(\boldsymbol{t}) \|^2 = \sum_{i=1}^{N} [r_{fq}(\Phi, t_i) - P_{fq}(t_i)]^2 \quad (7)$$

The objective function $J(\Phi)$ for the parameter optimization is formulated with the concatenated-frequencies method, which is the total SSE across all DBS frequencies:

$$J(\Phi) = SSE_{total}(\Phi) = \sum_{fq} SSE_{fq}(\Phi) \quad (8)$$

$J(\Phi)$ is minimized with the MATLAB custom function "*fminsearch*", which uses the Nelder – Mead simplex method [27,28] with the 5 variables in the parameter set Φ. Starting from an initial point $\Phi_0 = (\tau_0, r_{b,0}, c_0, s_0, k_0)$, the Nelder – Mead algorithm forms a simplex consisting of 6 vertices around Φ_0. Then the simplex is modified based on 5 operations: reflection, expansion, inside contraction, outside contraction and shrink. In the modified simplex, the algorithm searches for the vertex Φ_1 that minimizes the objective function $J(\Phi)$ and the next iteration starts from Φ_1. Compared with the traditional gradient-descent type optimization methods, the advantages of the the simplex method are (i) computation load is reduced because the derivative of the objective function is eliminated; and (ii) the searching direction is not restricted to the local gradient, and the algorithm can quickly approach the minimum in the first few iterations [28]. We implement the simplex method in "*fminsearch*" [28] to find the optimal parameter set $\Phi_{opt} = \{\tau_{opt}, r_{b,opt}, c_{opt}, s_{opt}, k_{opt}\}$ that minimizes the objective function $J(\Phi)$ defined in (8).

RESULTS

The Rate Model on Neuronal Dynamics across Multiple DBS Frequencies

We developed a firing rate model that can capture the dynamics of the neuronal activity of varying BGTCN nuclei across different DBS frequencies. Based on single-unit recordings of the neuron receiving DBS in a specific nuclei, we computed the reference firing rate with PSTH. Recordings across DBS frequencies were concatenated, and the optimal parameters were obtained by minimizing the distance to the reference PSTH firing rate (by Equation (8)) across all DBS frequencies using the Nelder – Mead simplex method [27,28]. **Figure 1** illustrates our rate model and the parameter optimization method.

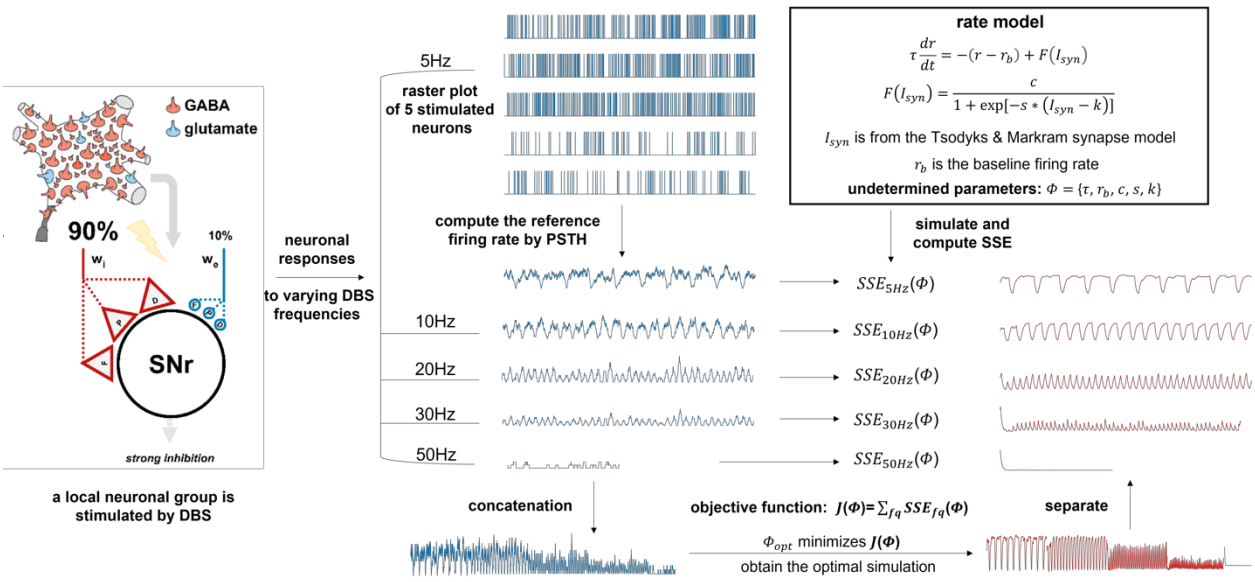

Figure 1. Schematic representation of the rate model (SNr - DBS as the example)

A local group of substantia nigra pars reticulata (SNr) neurons are stimulated by Deep Brain Stimulation (DBS) [10]. The 3 synapse types "F", "P", and "D" represent "facilitation", "pseudo-linear", and "depression", respectively. SNr neurons mostly receive the inhibitory gamma-aminobutyric acid (GABA) transmitter. For data from each DBS frequency, we computed the reference firing rate with peristimulus time histogram (PSTH) from the raster plot. Using the rate model, we performed independent simulations for each DBS frequency with the same parameter set $\emptyset$, and the objective function $J(\emptyset)$ is defined as the total sum of squared error (SSE). We then minimized $J(\emptyset)$ with the Nelder – Mead simplex method, and obtained the optimal parameter set $\emptyset_{opt}$. We simulated the rate model with $\emptyset_{opt}$ and obtain the optimal total fit, which minimizes the SSE from the concatenated PSTH firing rates. Finally, we separate the total fit and get the optimal fit for each DBS frequency.

Results — Synthetic Data

We compared firing rates of the rate model simulation with the synthetic data across different DBS frequencies in three different nuclei of the basal ganglia and thalamus, namely, Vim, STN, and SNr. For each nuclei, the synthetic data is the firing rate computed by PSTH with 20 simulated LIF model neurons (see **Materials and Methods**). **Figure 2** shows the model fitted firing rate (red) on top of the reference PSTH firing rate (black) for Vim, STN and SNr across different DBS

frequencies. We included a sample spike train of the LIF model neuron to better visualize the relationship between the PSTH and generated spikes.

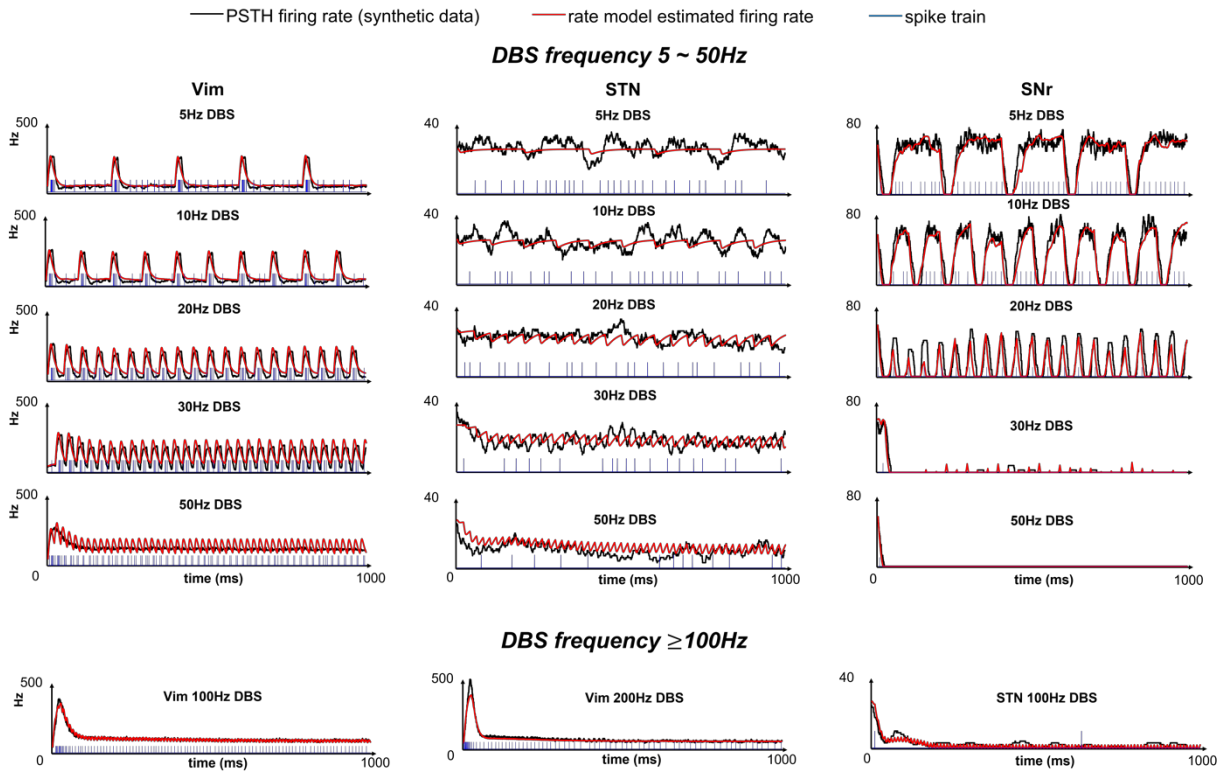

Figure 2. Rate model result for the synthetic data

The rate model is fitted to the synthetic data from the nuclei receiving Deep Brain Stimulation (DBS) in three basal ganglia and thalamic nuclei: ventralis intermedius (Vim), subthalamic nucleus (STN), and substantia nigra pars reticulate (SNr). The synthetic data are the simulated membrane potentials from the leaky integrate-and-fire (LIF) model in Milosevic et al. [10]. We compare the firing rate computed by peristimulus time histogram (PSTH) from the synthetic data, firing rate predicted by our rate model and the spike timings from one spike train. DBS stimuli with varying pulse frequencies (5~200Hz) are delivered to the related basal ganglia and thalamic nuclei. The data from stimulated nuclei receiving lower frequency DBS (5~50Hz) are recorded in all three nuclei, whereas higher frequency DBS (≥100Hz) is delivered to Vim and STN.

As can be seen in **Figure 2**, the estimated instantaneous firing rate reliably matched the PSTHs generated by ensemble of spiking neurons for all four different nuclei and across all DBS

frequencies. In addition, both the steady-state and transient part of the neurons' firing rate were replicated using the rate model.

It should be noted that the conventional approach for modeling DBS-evoked neural response—regardless the optimization technique or the modeling framework—were based on data recorded from a single DBS frequency [21], ignoring frequency-dependent behavior of DBS neural responses. High frequency DBS was often used to fit the model [21]; however, therapeutic effective DBS frequencies are often undetermined and depend on individual situations [36,37,10]. In some certain case studies, the effective DBS frequencies are ~130Hz for Vim [38], ≥100Hz for STN [39] and below 70Hz for SNr [40]. Unlike other studies, we developed a "concatenated-frequencies method" in optimizing model parameters, by incorporating the contribution of various DBS frequencies in our rate model and estimated model parameters that are consistent across those frequencies. The concatenated-frequencies method includes all the previously mentioned DBS frequencies, i.e., {5, 10, 20, 30, 50, 100, and 200Hz} (for STN and SNr, the maximum is 100Hz and 50Hz, respectively). To compare the concatenated-frequencies method with the parameter estimation based on only a single DBS frequency ("single-frequency method"), we fit our model using a single DBS frequency for Vim-DBS = 100Hz, STN-DBS = 100Hz and SNr-DBS = 20Hz; the comparison result is shown in **Figure 3**. For both optimization methods, we used the estimated model parameters to replicate the firing rate for 24 observed and unobserved DBS frequencies in 0~200 Hz, including {2.5, 5, 7.5, 10, 15, 20, 30, 40, 50, 60, 70, 80, 90, 100, 110, 120, 130, 140, 150, 160, 170, 180, 190, and 200Hz} (for STN and SNr, the maximum is 100Hz and 50Hz, respectively). We used the normalized mean squared error (NMSE) to measure the error between the estimated firing rate and the reference firing rate computed by PSTH. **Figure 3**(**A**) shows a sample of estimated firing rates using single-frequency and concatenated-frequencies methods for Vim. For

the parameter estimation based on a single DBS frequency, model parameters were obtained from Vim-DBS = 100Hz and the estimated firing rate was plotted for DBS of 5Hz & 100Hz. The estimated firing rate based on a single DBS frequency worked well for that frequency but failed for the other (5Hz). However, the estimated firing rate based on multiple DBS frequencies reliably reproduced both the transient- and steady-states of the instantaneous firing rate. For the parameter estimation based on a single DBS frequency, we observed (data not shown) that the estimated firing rate could only replicate the original instantaneous firing rates for DBS frequencies of 100Hz and 50Hz; it produced large deviations for smaller DBS frequencies.

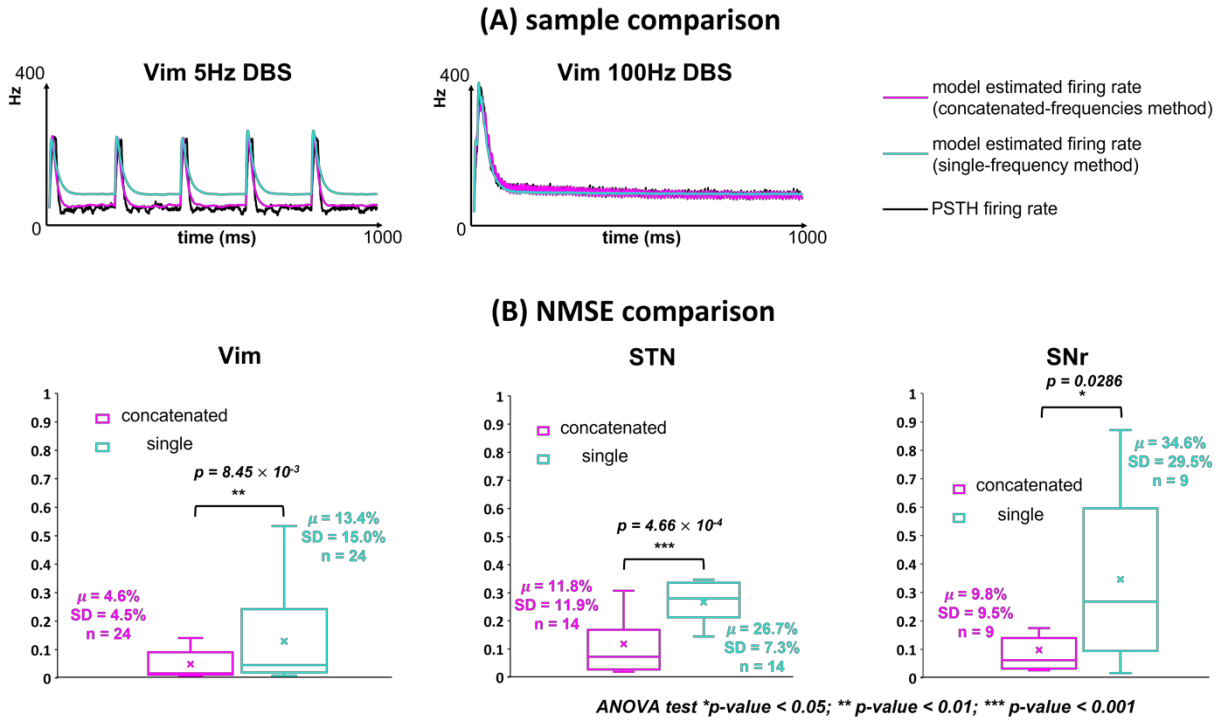

Figure 3. Comparison of two optimization methods in the rate model

"Single-frequency" and "concatenated-frequencies" optimization methods are compared for three basal ganglia and thalamic nuclei: ventralis intermedius (Vim), subthalamic nucleus (STN), and substantia nigra pars reticulate (SNr). (A) The two plots compare the prediction results of the two methods on Vim with varying DBS frequencies. We compare the firing rate computed by peristimulus time histogram (PSTH), and the firing rate predicted by our rate

model with each of the two optimization methods. PSTH firing rate is computed based on the synthetic data, i.e., the simulated spike trains of the spiking model in Milosevic et al. [10]. For Vim, data from 100Hz DBS is used to train model parameters in the single-frequency method. (B) Normalized mean squared error (NMSE) of the model prediction of multiple DBS frequencies (see text for details) is calculated based on the reference PSTH firing rate. The NMSE results are presented with the box-whisker plot; "concatenated" and "single" mean concatenated-frequencies method and single-frequency method, respectively. "μ" represents the mean value, "SD" represents the standard deviation, and "n" represents the number of samples. ANOVA represents "the one-way analysis of variance test".

The NMSE calculated using single and multiple DBS frequencies were shown in **Figure 3**(**B**) for all nuclei. The NMSE's calculated by multiple DBS frequencies were significantly smaller (with regard to mean and standard deviation) than those obtained by a single DBS frequency. For the parameter estimation based on multiple DBS frequencies, the mean NMSE for Vim, STN and SNr is 4.6%, 11.8% and 9.8%, respectively; the standard deviation of NMSE for Vim, STN and SNr is 4.5%, 11.9% and 9.5%, respectively. The small NMSE compared to that based on single DBS frequency indicates that our proposed rate model with the concatenated-frequencies optimization method could much better reproduce the PSTH firing rate (ANOVA, $p < 0.05$ for all nuclei; $p = 8.45 \times 10^{-3}$ for Vim, $p = 4.66 \times 10^{-4}$ for STN, $p = 0.0286$ for SNr). It is worth mentioning that the low NMSE of the parameter estimation based on multiple (observed) frequencies was obtained across all observed and unobserved frequencies, confirming the generalizability of the proposed model and the consistency of estimated parameters. We anticipate that such a reliable predictive model can be used in clinical applications and it outperforms trial-and-error DBS frequency selection processes [9,12].

Results — Experimental Data

To test the potential of the rate model to reproduce instantaneous firing rate of an ensemble of neurons recorded from human brain during DBS, we fit the rate model to experimental data obtained from single-unit recordings [10] on three different nuclei of basal ganglia and thalamus: Vim, STN, and SNr. To calculate the firing rate of an ensemble of neurons for each nuclei, spikes recorded from 5 to 8 different individuals were combined, and the instantaneous firing rate was then obtained by calculating the PSTH. Similar to the results for the synthetic data, we estimated model parameters that fit the rate model output to the PSTH. **Figure 4** shows the results of the fit model output with the PSTH for different nuclei and different DBS frequencies.

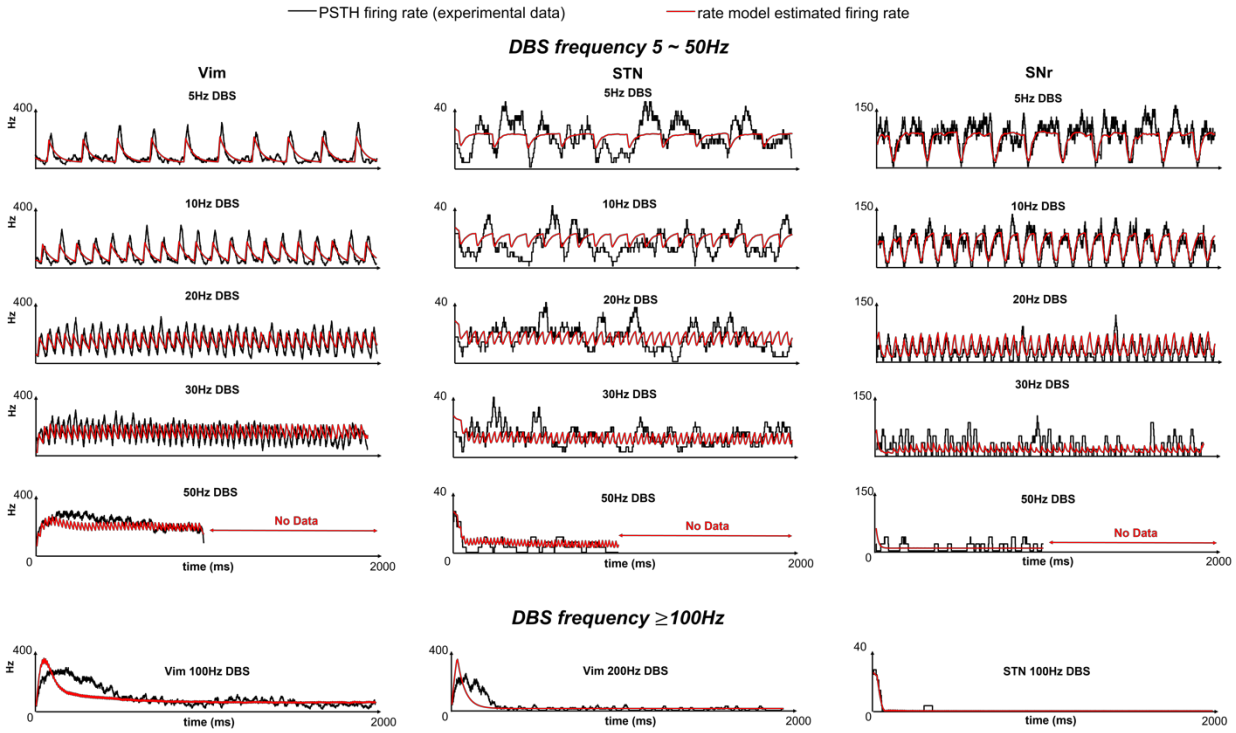

Figure 4. Rate model result for the experimental data

The rate model is fitted to the experimental data (single-unit recordings) from the nuclei receiving Deep Brain Stimulation (DBS) in three basal ganglia and thalamic nuclei: ventralis intermedius (Vim), subthalamic nucleus (STN), and substantia nigra pars reticulate (SNr). We compare the firing rate computed by peristimulus time histogram (PSTH)

from the experimental data and the firing rate predicted by our rate model. The experimental data are from single-unit DBS recordings in the specific basal ganglia and thalamic nuclei. The recording length for 50 Hz DBS data is ~1s. The data from stimulated nuclei receiving lower frequency DBS (5~50Hz) are recorded in all 3 nuclei, whereas higher frequency DBS (≥100Hz) is delivered to Vim and STN.

Firing rates estimated by the rate model track both transient- (mostly apparent for DBS frequencies ≥30 Hz) and steady-state components of PSTHs of all nuclei. The NMSE computed based on the concatenated signal from all DBS frequencies for Vim, STN and SNr is 14.1%, 18.1% and 9.5%, respectively. However, the rate model could not reproduce the transient response of the Vim for DBS frequencies of 100 Hz and 200 Hz as accurately as it could for other nuclei. The rate model generated a shorter transient response compared to that observed in experimental recordings. This mismatch between transient responses might be originated from network effects and is further addressed in **Discussions**.

Physiological Implications of the Model Parameters

The optimal rate model parameters, $\Phi_{opt} = \{\tau_{opt}, r_{b,opt}, c_{opt}, s_{opt}, k_{opt}\}$, of each nuclei, for both synthetic and experimental data, are listed in **Table 1**:

Table 1: Rate model optimal parameters (3 significant figures)

source	site	τ_{opt}	$r_{b,opt}$	c_{opt}	s_{opt}	k_{opt}
synthetic data	Vim	10.4	10.0	433	4.40×10^{-3}	616
	STN	36.0	27.5	-51.5	-0.470	-14.0
	SNr	11.1	77.1	-96.6	-0.273	-17.8
	Rt	11.9	2.53	392	3.20×10^{-2}	112

experimental data	Vim	45.1	13.4	687	5.81×10^{-2}	548
	STN	24.7	27.6	-34.4	-0.425	-5.42
	SNr	11.5	95.3	-88.6	-0.236	-21.5
	Rt	32.2	3.00	578	32.9	53.3

The optimal model parameters are in distinct ranges for different nuclei of the basal ganglia and thalamus. For the same nuclei, the optimal parameters of synthetic and experimental data are generally similar but differences exist. The combination of these abstract parameters forms the firing rate response to the input synaptic current I_{syn} through the sigmoid function as defined in (6): $\tau \frac{dr}{dt} = -(r - r_b) + F(I_{syn})$, $F(I_{syn}) = \frac{c}{1+\exp[-s*(I_{syn}-k)]}$. To better assess the effect of these parameters on the rate model, we plotted the model estimated firing rate (r) versus I_{syn} in **Figure 5** to detect the firing rate dynamics of each nuclei across varying DBS frequencies. In other words, this figure describes the *f-I* curve for each nuclei receiving DBS. The *f-I* curve was created by the estimated parameters in **Table 1** for both synthetic and experimental data. The firing rate and I_{syn} were ordered according to their percentiles (from 0 to 100), and the percentiles were matched at each point in the curve to qualitatively represent the relationship between the firing rate and input current [41,42]. A similar curve was created in Lim et al. [43] for the rate network model to calculate the current-rate transfer function. In our proposed model, see (6), the sigmoid transfer function $F(I_{syn})$ models the firing rate variability caused by the input synaptic current (I_{syn}); see **Supplementary Figure 1** for $F(I_{syn})$ in each nuclei across different DBS frequencies.

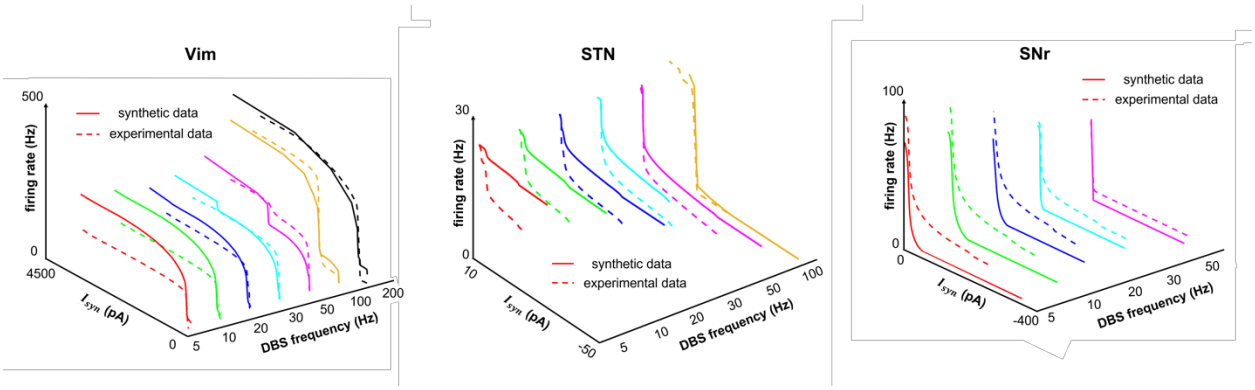

Figure 5. Rate model estimated firing rate in response to the input synaptic current

The rate model is fitted to both synthetic and experimental data; the synthetic data are from the spiking model in Milosevic et al. [10], and the experimental data are single-unit recordings. We present the model fits across all Deep Brain Stimulation (DBS) frequencies, in each of the three basal ganglia and thalamic nuclei: ventralis intermedius (Vim), subthalamic nucleus (STN), and substantia nigra pars reticulate (SNr). We plot the relationship between the rate model estimated firing rate and the simulated input synaptic current (I_{syn}) to the nuclei receiving DBS. Each point in a curve represents that the corresponding firing rate and the input synaptic current have the same percentile (in the range 0 to 100).

In **Figure 5**, the model estimated firing rate monotonically increases as the input synaptic current becomes more excitatory or less inhibitory, in both synthetic and experimental data. Note that the minus sign of I_{syn} indicates inhibition and the positive sign denotes excitation. For SNr and STN with predominantly inhibitory inputs, the *f-I* curve is monotonically decreasing, across all DBS frequencies, indicating that neurons in this nuclei receive more inhibitory synaptic inputs when DBS is ON. When DBS is active, the firing rate quickly drops from its baseline value given negative net current received by SNr neurons. The slope of this fast decay is facilitated in higher frequencies of DBS. Unlike SNr neurons that receive more inhibitory synaptic inputs given DBS pulses, the firing rate of Vim neurons increase monotonically with respect to total synaptic current whose net effect is positive when DBS is ON. The slope of the *f-I* curve increases for higher

frequencies of DBS in Vim neurons. One can note that in experimental and synthetic data, for each nuclei, the calculated *f-I* curves (**Figure 5**) are generally similar, although some differences exist. The differences between the *f-I* curves in experimental and synthetic data (**Figure 5**) are mostly not from the rate model fits in this work, but mainly lie in the mismatch between the experimental data and simulation of the LIF model in Milosevic et al. [10].

DISCUSSIONS

In this paper, we developed a firing rate model on three BGTCN nuclei receiving DBS: Vim, STN and SNr. With our rate model, we have accurately reproduced the firing rate dynamics obtained from both synthetic and experimental data. Compared with the spiking network models [44,20], the firing rate model is much faster and more robust in implementations, because of the fewer number of equations and lower dimensionality in model parameters [45]. We also developed a concatenated-frequencies optimization method that systematically computes the optimal model parameters that are fitted across different DBS frequencies. Compared with the manual parameter tuning in Milosevic et al. [10], the optimization method in this work can systematically and automatically compute the model parameters, so it is conveniently implementable in practice. Since the same set of model parameters can be implemented across varying DBS frequencies, we can potentially use the model to target the optimal DBS frequency with the maximal clinical benefits, without extensive additional experimental data recordings constrained by the patients' consents [9].

Other Methods for Modeling Firing Rate

Various firing rate models have been developed to infer physiological mechanisms underlying neuronal networks [16,43,46]. Lim et al. [43] developed a rate model on the recurrent network of the monkey visual cortex, and investigated the learning rules that differentiate novel and familiar external visual stimuli; the result is in good consistency with experimental data. Murphy et al. [46] developed a rate model on a general recurrent network consisting of interacting excitatory and inhibitory nuclei, and investigated the role of inhibitory nuclei in balancing the firing rates of strongly coupled excitatory neurons receiving external stimuli.

In modeling neuronal firing rate, one critical challenge is to appropriately transfer the postsynaptic input current to the corresponding firing rate variability. In our model, we used a sigmoid function to transfer the impact of filtered (by synaptic model) DBS to a firing rate model ODE (Equation (6)). Our approach for computing firing rate with the sigmoid-ODE is significantly more accurate than the commonly implemented simplified approach, which obtains firing rate directly from the average membrane potential through a transfer function [47184849] (see **Supplementary Figure 3**). In **Supplementary Method B**, we constructed a typical method on computing firing rate directly from the average membrane potential, and this alternative method was compared with our model.

Further Discussions on Model Physiological Implications

For Vim neurons, the large excitatory I_{syn} (**Figure 5**) is caused by the high proportion of glutamate pre-synapses [10], which induces fast changes of the firing rates. In general, the firing rate increases as we stimulate with higher DBS frequency. The modeled firing rate from either

experimental or synthetic data (**Figure 5**) has similar patterns (across different DBS frequencies) based on the amplitude of I_{syn}: (i) When I_{syn} is small, the firing rate increases quickly as the excitatory input increases; (ii) When I_{syn} is large, the firing rate slowly increases and finally saturates as I_{syn} increases. This probably indicates that when the input excitatory postsynaptic current (I_{syn}) is strong, the increase of firing rate is restricted due to the limited amount of ions to support the neuronal firing.

For SNr (**Figure 5**), we see that the firing rate is low and close to zero in most of the range of I_{syn}, in both experimental and synthetic data across all DBS frequencies. The modeled firing rate (**Figure 5**) has similar patterns (across different DBS frequencies) based on the I_{syn} amplitude: (i) When the inhibition is strong (i.e., large I_{syn} amplitude), the firing rate is low and mostly close to 0; (ii) When the inhibition is removed (i.e., $I_{syn} \sim 0$), the firing rate returns to the baseline at ~60Hz [10]. The large inhibitory I_{syn} is consistent with the high proportion (~90%) of gamma-aminobutyric acid (GABA) pre-synapses of SNr neurons [10].

In **Supplementary Figure 1**, we can see that the sigmoid nonlinearity $F(I_{syn})$ in response to I_{syn} is generally similar between synthetic and experimental data for each of the three BGTCN nuclei (Vim, STN and SNr). For each nuclei, the differences between $F(I_{syn})$ in experimental and synthetic data (**Supplementary Figure 1**) are mostly not from the rate model fits in this work, but mainly lie in the mismatch between the experimental data and simulation of the LIF model in Milosevic et al. [10]. For SNr and STN (dominant inhibitory), $F(I_{syn})$ is mostly negative with the evidently inhibitory I_{syn}. For Vim, as I_{syn} increases, $F(I_{syn})$ first increases then plateaus; this indicates that the increase of the firing rate is restricted due to the limitation of ions, although the

postsynaptic current (I_{syn}) is large [13]. Since I_{syn} incorporates the STP rules in the synapse, $F(I_{syn})$ partially reflects the firing rate regulation of the neuron beyond the synaptic contacts.

Limitations and Future Work

Our model represents local groups of neurons, but we did not model the network interactions among the connected neuronal groups. For example, the afferent synaptic connections to Vim neurons consist of both excitatory and inhibitory effects [11]. For a Vim neuron, the excitatory pre-synapses are mainly from the cortex and the cerebellum [10], and the inhibitory pre-synapses are mainly from Rt and the interneurons [50,51]. We modelled the local Vim neurons receiving DBS, whereas the DBS-induced upsteam / downsteam network effects from other nuclei are not included in the model.

From **Figure 4** (experimental data, Vim), we see that the firing rate prediction with our model is not very accurate at high DBS frequencies (100Hz and 200Hz). In Vim experimental data at high frequency DBS, the initial transient large firing rate response (~400ms) is clearly longer than the model simulation (~200ms). We hypothesize that the model firing rate predictions in response to DBS at high frequencies can be better explained if we include network effects into the rate model in this work.

From the experimental data fit of STN in **Figure 4**, we observe that our model misses some firing rate oscillations, in particular for the 5Hz & 10Hz DBS data. The oscillation in STN nuclei is mainly caused by interaction of inputs from the cortex [52] and the external globus pallidus (GPe) [53]. In particular, the STN-GPe recurrent network contributes much to the oscillatory behaviors in STN [53,54]. Thus, in order to completely model the firing rate oscillations in STN, the single ODE model in this work may not be sufficient. However, although the current model focuses on a single

STN population, the fitting error is small; the average NMSE across varying DBS frequencies is 11.8% for the synthetic data (**Figure 3**), and 18.1% for the experimental data (**Figure 4**). We anticipate that the fitting accuracy will be improved in our future work by incorporating the network effects and oscillations.

The synaptic input to STN neurons is diverse; some STN neurons receive predominantly excitatory whereas other STN neurons receive predominately inhibitory inputs [10,33,55]. In this work, we only modelled STN nuclei with dominant inhibitory inputs, that have been shown to be persistent at high frequency both in rat [55] and human [33]. In the future work, we aim to incorporate STN neurons that receive predominantly excitatory synapses, that have been shown to be governed by different short-term synaptic depression (STD) dynamics than inhibitory inputs to STN [55]. Furthermore, incorporating both dynamics of inhibitory and excitatory inputs to STN will help us predict the firing rate oscillations in the STN and its (sub-)cortical network.

In clinical applications, the appropriate choice of DBS parameters, in particular the DBS frequency, is critical for successful therapeutic results and reducing side effects [9,56]. However, the process of choosing DBS parameters relies largely on inefficient trial-and-error approaches that are based on neurologist experience and clinical observations [9,11,12]. Based on the relationship between neuronal pathological firing rates and the disease symptoms, our rate model has a potential to provide a quantitative method for choosing the optimal DBS frequency that is therapeutically effective (i.e., symptom relieving). The determination of the optimal DBS parameters depends on the further understanding of the neuronal network mechanisms underlying the disease and the therapeutic effects of DBS [11]. It is noted that we focused on tuning DBS frequencies in this work; although the DBS frequency is the most commonly tuned parameter in clinical applications [10,39], the optimization of other DBS parameters (e.g., pulse width and

amplitude) may also contribute to a better clinical performance. Even with the limitations in not modeling DBS pulse width and amplitude, our model fits the clinically recorded experimental data consistently across varying DBS frequencies, for each BGTCN nuclei (STN, SNr, Vim and Rt).

Conclusion

In this paper, we developed a firing rate model on the basal ganglia and thalamic neurons receiving DBS. We developed a concatenated-frequencies optimization method that computes the consistent model parameters fitted across different DBS frequencies. Our model can accurately reproduce the firing rate obtained from both synthetic data and experimental single-unit recordings. Such consistency and accuracy of the model fits demonstrate that our model can be potentially implemented in optimizing the DBS frequency, and improving the clinical performances of DBS.

Data Availability Statement

The human experimental datasets and codes have not been deposited in a public repository due to restrictions related to the ethics protocol, but the data and codes are available from the corresponding author upon request and completion of a data transfer agreement.

SUPPLEMENTARY INFORMATION

Supplementary Method A — The Leaky Integrate-and-Fire (LIF) Spiking Model

The LIF model in Milosevic et al. [10] was implemented to generate the synthetic data used in our analysis. In this LIF model, the total input current (I_{total}) to a stimulated neuron consists of two components: the post-synaptic current (I_{syn}) and background noise (I_{noise}), i.e.

$$I_{total} = I_{syn} + I_{noise} \tag{9}$$

I_{syn} is obtained with the Tsodyks & Markram model formulated in **Materials and Methods**. I_{noise} is modeled by the Ornstein-Uhlenbeck (OU) process with time constant of 5ms [57], and is written as:

$$\frac{dI_{noise}}{dt} = -\frac{I_{noise}(t)-\mu}{\tau} + \mathrm{a}\sqrt{\frac{2}{\tau}}\frac{\xi(t)}{\sqrt{dt}} \tag{10}$$

where $\xi(t)$ is white noise with mean = 0 and variance = 1. $\tau = 5$ms is the time constant, μ and a indicate the mean and standard deviation of I_{noise}, respectively. $\{\mu, \mathrm{a}\}$ is different for each BGTCN nuclei; the different values are shown in **Supplementary Table 5**.

The dynamics of the membrane potential of a stimulated neuron in an LIF model can be written as:

$$\frac{dV(t)}{dt} = \frac{-(V(t)-E_L)+R*I_{total}(t)}{\tau_V} \tag{11}$$

where $E_L = -70$mV is the equilibrium potential, R (scaling parameter) = 1, and τ_V (membrane time constant) = 10ms. I_{total} is the total input current (Equations (9) – (10)). Spikes occur when $V \geq V_{th}$, for $V_{th} = -40$mV. The reset voltage is -90mV and the absolute refractory period is 1ms.

Supplementary Method B — Alternative Approach to Model Instantaneous Firing Rate

Different from our rate model, the commonly used simplified approach to obtain firing rate is by directly implementing a transfer function from the average membrane potential [47,18,48,49]. We construct such an alternative method by modeling the average membrane potential ($\bar{V}$), and then implementing a sigmoid transfer function [47,18].

We fit the alternative method to the same synthetic data as in **Materials and Methods**. In the synthetic data, we assumed that DBS is delivered to a local group of homogeneous LIF neurons, and the average membrane potential ($\bar{V}$) of this homogeneous group is modeled with the following equations:

$$\frac{d\bar{V}(t)}{dt} = \frac{-(\bar{V}(t)-E_L)+R*I_{total}(t)}{\tau_V}\,;\, I_{total} = I_{syn} + I_{noise} \tag{12}$$

where I_{total} is the total input current computed with Equations (9) – (10). Compared with the model of an individual neuron with Equation (11), the parameters related to Equation (12) are determined as follows: (i) The standard deviation (= a) of I_{noise} in Equation (10) is reduced to $\frac{a}{\sqrt{50}}$ to compute the variability of $\bar{V}$ on ~50 representative stimulated local homogeneous neurons [58]; (ii) In terms of the amplitude of membrane potential, the average value ($\bar{V}$) needs to be consistent with each individual LIF neuron. Thus, we tuned the scaling parameter R to be 0.07, so that the mean of the $\bar{V}$ simulation with Equation (12) is consistent with the mean membrane potential obtained from simulating a single LIF neuron with Equation (11); (iii) All the remaining parameters are the same as the model of an individual neuron with Equation (11).

After modeling the average membrane potential ($\bar{V}$), we obtain the firing rate directly from $\bar{V}$ through a sigmoid transfer function:

$$r(t) = \frac{\theta}{1+\exp\left[-s*(\bar{V}-k)\right]} \tag{13}$$

In (13), the undetermined parameter set is $\emptyset = \{\theta, s, k\}$; we optimize $\emptyset$ with the same concatenated-frequencies optimization method (see **Materials and Methods**) as in our rate model. This alternative approach to obtain the instantaneous firing rate is compared with our rate model using Vim synthetic data (**Supplementary Figure 3**).

In **Supplementary Figure 3**, we see that the alternative approach has large deviations in synthetic data from both low-frequency and high-frequency DBS on Vim. The firing rate amplitude is not captured in both 10Hz and 100Hz DBS, and the transient response (initial ~200ms) in 100Hz DBS is much longer than the reference (PSTH firing rates). In terms of the NMSE of 24 varying DBS frequencies {2.5, 5, 7.5, 10, 15, 20, 30, 40, 50, 60, 70, 80, 90, 100, 110, 120, 130, 140, 150, 160, 170, 180, 190, and 200Hz}, the alternative approach is significantly larger than our rate model (ANOVA, $p = 8.99 \times 10^{-9}$). Thus, the alternative approach is not sufficient for reproducing firing rate dynamics; our rate model is the more sophisticated approach, and is efficient in detecting the firing rate mechanism consistent across various DBS frequencies.

Supplementary Table 1 – Proportions of excitatory and inhibitory synapses

	number of excitatory synapses	**number of inhibitory synapses**
STN	150 (30%)	350 (70%)
SNr	50 (10%)	450 (90%)
Vim / Rt	450 (90%)	50 (10%)

Supplementary Table 2 – Weights & time constants of excitatory and inhibitory synaptic currents in I_{syn}

	w_{exc}	w_{inh}	τ_{exc} (ms)	τ_{inh} (ms)
STN	1.2	1	3	5
SNr	6	4	3	10
Vim	37.5	90	5	8.5
Rt	4.37	11.4	5	8.5

Supplementary Table 3 – the three types of excitatory synapses

(A). Parameters

	facilitation			**depression**			**pseudo linear**		
	τ_D (ms)	τ_F (ms)	U	τ_D (ms)	τ_F (ms)	U	τ_D (ms)	τ_F (ms)	U
STN, SNr, Vim / Rt	138	670	0.09	671	17	0.5	329	326	0.29

(B). The ratio of excitatory synaptic types

	facilitation	**depression**	**pseudo linear**
STN	0.1	0.6	0.3
SNr	0.3	0.4	0.3
Vim	0.5	0.3	0.2
Rt	0.5	0.3	0.2

Supplementary Table 4 – the three types of inhibitory synapses

(A). Parameters

	facilitation			**depression**			**pseudo linear**		
	τ_D **(ms)**	τ_F **(ms)**	U	τ_D **(ms)**	τ_F **(ms)**	U	τ_D **(ms)**	τ_F **(ms)**	U
STN, SNr, Vim / Rt	45	376	0.016	706	21	0.25	144	62	0.29

(B). The ratio of inhibitory synaptic types

	facilitation	**depression**	**pseudo linear**
STN	0.4	0.3	0.3
SNr	0.3	0.4	0.3
Vim	0.3	0.4	0.3
Rt	0.3	0.4	0.3

Supplementary Table 5 – Parameters of the background noise current I_{noise} (in pA) in the LIF model [10]

	mean (μ)	**st. dev. (a)**
STN	32	11
SNr	55	10
Vim	30	45
Rt	12	10

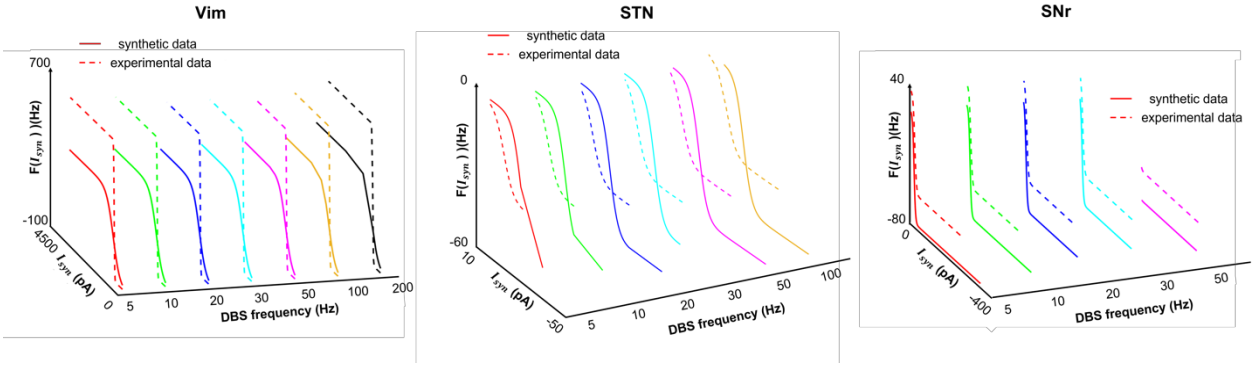

Supplementary Figure 1. Sigmoid nonlinearity in response to the input synaptic current

The firing rate variability caused by the input synaptic current is modeled by the sigmoid transfer function (Equation (6)). We present the transfer functions in both synthetic and experimental data; the synthetic data are from the spiking model in Milosevic et al. [10], and the experimental data are single-unit recordings. We show the transfer functions across all Deep Brain Stimulation (DBS) frequencies, in each of the three basal ganglia and thalamic nuclei: ventralis intermedius (Vim), subthalamic nucleus (STN), and substantia nigra pars reticulate (SNr).

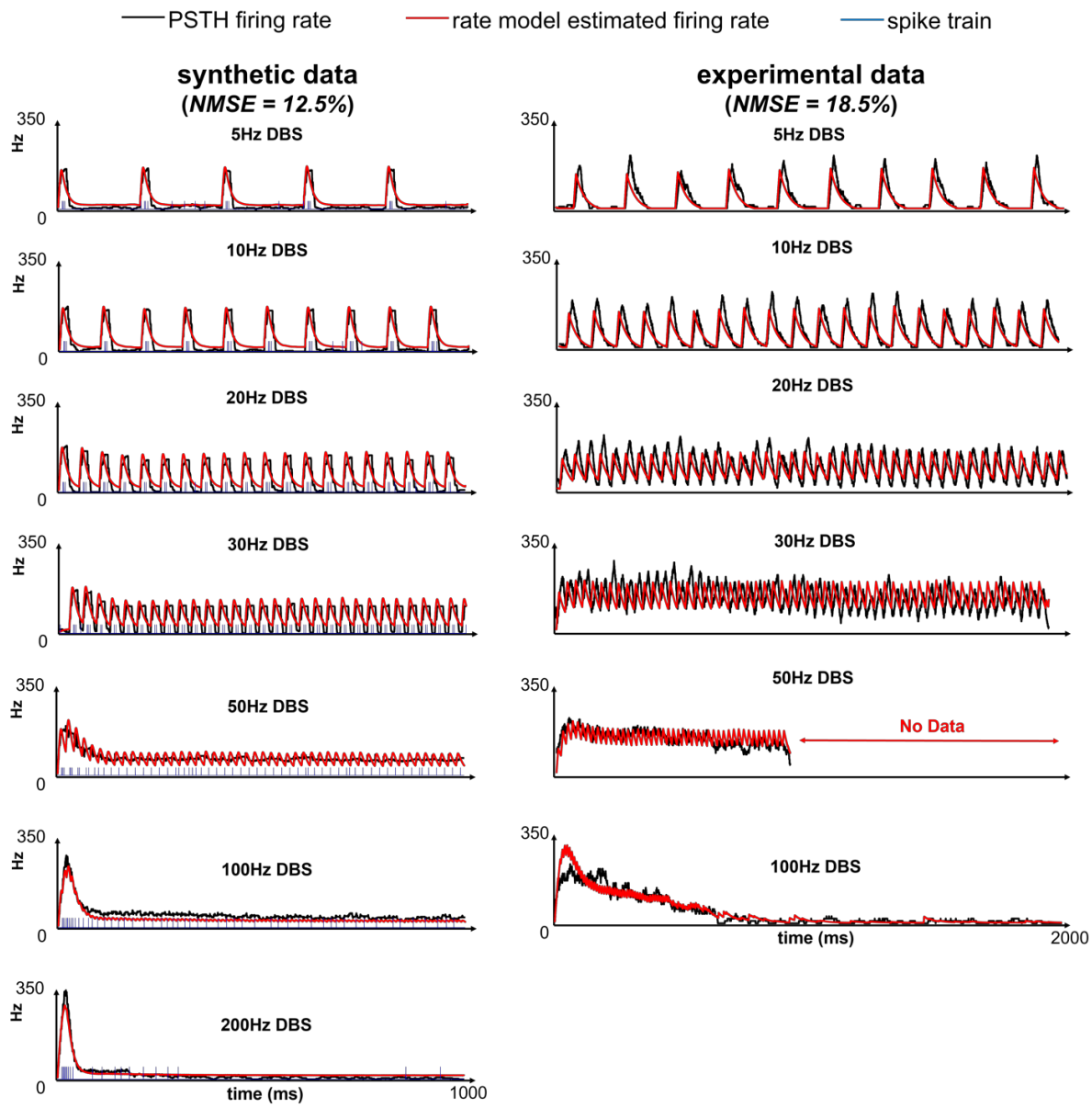

Supplementary Figure 2. Rate model results for Rt

The rate model is fitted to both synthetic and experimental data from reticular thalamic nucleus (Rt) receiving Deep Brain Stimulation (DBS). The synthetic data are the simulated membrane potentials from the leaky integrate-and-fire (LIF) model established in Milosevic et al. [10], and the experimental data are the single-unit recordings. We compare the firing rate computed by peristimulus time histogram (PSTH), firing rate predicted by our rate model and the spike timings

from one spike train (for synthetic data only). DBS stimuli with varying pulse frequencies are delivered, and the normalized mean squared error (NMSE) is computed based on the concatenated signal from all DBS frequencies.

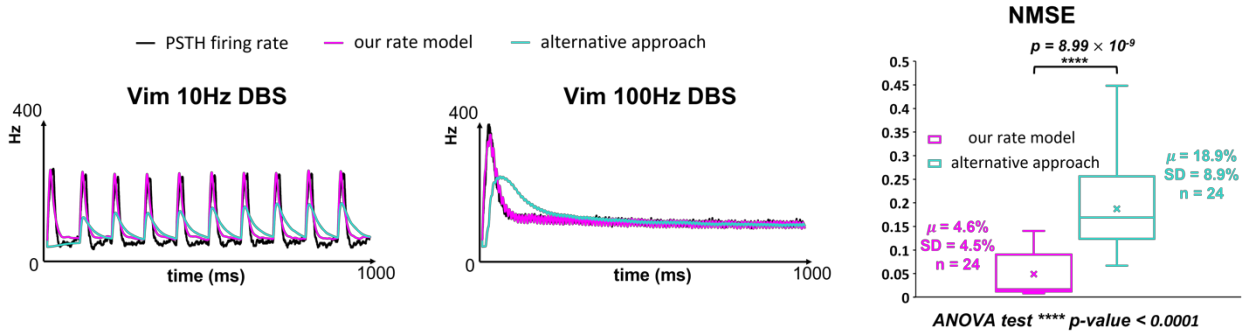

Supplementary Figure 3. Comparison of our rate model with an alternative approach

We compare our rate model with the alternative approach (**Supplementary Method B**) of obtaining firing rate, in the synthetic data on ventralis intermedius (Vim). The synthetic data are the simulated membrane potentials from the leaky integrate-and-fire (LIF) model in Milosevic et al. [10]. The alternative approach represents that the firing rate is obtained directly from the average membrane potential through a sigmoid transfer function (**Supplementary Method B**). Normalized mean squared error (NMSE) is based on the ground truth firing rate computed by the peristimulus time histogram (PSTH) with the synthetic data. NMSE is compared based on data from the same set of DBS frequencies as in **Figure 3** (also see text), and presented with the box-whisker plot. "μ" represents the mean value, "SD" represents the standard deviation, and "n" represents the number of samples. ANOVA represents "the one-way analysis of variance test".

REFERENCES

1. Lebouvier T, Chaumette T, Paillusson S, et al. The second brain and Parkinson's disease. *Eur J Neurosci*. 2009;30(5):735-741. doi:10.1111/j.1460-9568.2009.06873.x

2. van Albada SJ, Gray RT, Drysdale PM, Robinson PA. Mean-field modeling of the basal ganglia-thalamocortical system. II Dynamics of parkinsonian oscillations. *J Theor Biol*. 2009;257(4):664-688. doi:10.1016/j.jtbi.2008.12.013

3. Limousin P, Krack P, Pollak P, et al. Electrical Stimulation of the Subthalamic Nucleus in Advanced Parkinson's Disease. *New England Journal of Medicine*. 1998;339(16):1105-1111. doi:10.1056/NEJM199810153391603

4. Dallapiazza RF, Lee DJ, Vloo PD, et al. Outcomes from stereotactic surgery for essential tremor. *J Neurol Neurosurg Psychiatry*. 2019;90(4):474-482. doi:10.1136/jnnp-2018-318240

5. Hung SW, Hamani C, Lozano AM, et al. Long-term outcome of bilateral pallidal deep brain stimulation for primary cervical dystonia. *Neurology*. 2007;68(6):457. doi:10.1212/01.wnl.0000252932.71306.89

6. Menchón JM, Real E, Alonso P, et al. A prospective international multi-center study on safety and efficacy of deep brain stimulation for resistant obsessive-compulsive disorder. *Molecular Psychiatry*. Published online October 29, 2019:1-14. doi:10.1038/s41380-019-0562-6

7. Laxton AW, Lozano AM. Deep Brain Stimulation for the Treatment of Alzheimer Disease and Dementias. *World Neurosurgery*. 2013;80(3):S28.e1-S28.e8. doi:10.1016/j.wneu.2012.06.028

8. Fisher R, Salanova V, Witt T, et al. Electrical stimulation of the anterior nucleus of thalamus for treatment of refractory epilepsy. *Epilepsia*. 2010;51(5):899-908. doi:10.1111/j.1528-1167.2010.02536.x

9. Boutet A, Madhavan R, Elias GJB, et al. Predicting optimal deep brain stimulation parameters for Parkinson's disease using functional MRI and machine learning. *Nature Communications*. 2021;12(1):3043. doi:10.1038/s41467-021-23311-9

10. Milosevic L, Kalia SK, Hodaie M, et al. A theoretical framework for the site-specific and frequency-dependent neuronal effects of deep brain stimulation. *Brain Stimulation*. 2021;14(4):807-821. doi:10.1016/j.brs.2021.04.022

11. Yousif N, Mace M, Pavese N, Borisyuk R, Nandi D, Bain P. A Network Model of Local Field Potential Activity in Essential Tremor and the Impact of Deep Brain Stimulation. *PLoS Comput Biol*. 2017;13(1). doi:10.1371/journal.pcbi.1005326

12. Picillo M, Lozano AM, Kou N, Puppi Munhoz R, Fasano A. Programming Deep Brain Stimulation for Parkinson's Disease: The Toronto Western Hospital Algorithms. *Brain Stimul*. 2016;9(3):425-437. doi:10.1016/j.brs.2016.02.004

13. Rosenbaum R, Zimnik A, Zheng F, et al. Axonal and synaptic failure suppress the transfer of firing rate oscillations, synchrony and information during high frequency deep brain stimulation. *Neurobiol Dis*. 2014;62:86-99. doi:10.1016/j.nbd.2013.09.006

14. Farokhniaee A, McIntyre CC. Theoretical principles of deep brain stimulation induced synaptic suppression. *Brain Stimul*. 2019;12(6):1402-1409. doi:10.1016/j.brs.2019.07.005

15. Jercog D, Roxin A, Barthó P, Luczak A, Compte A, Rocha J de la. UP-DOWN cortical dynamics reflect state transitions in a bistable network. eLife. doi:10.7554/eLife.22425

16. Hennequin G, Ahmadian Y, Rubin DB, Lengyel M, Miller KD. The Dynamical Regime of Sensory Cortex: Stable Dynamics around a Single Stimulus-Tuned Attractor Account for Patterns of Noise Variability. *Neuron*. 2018;98(4):846-860.e5. doi:10.1016/j.neuron.2018.04.017

17. Dipoppa M, Ranson A, Krumin M, Pachitariu M, Carandini M, Harris KD. Vision and Locomotion Shape the Interactions between Neuron Types in Mouse Visual Cortex. *Neuron*. 2018;98(3):602-615.e8. doi:10.1016/j.neuron.2018.03.037

18. van Albada SJ, Robinson PA. Mean-field modeling of the basal ganglia-thalamocortical system. I Firing rates in healthy and parkinsonian states. *J Theor Biol*. 2009;257(4):642-663. doi:10.1016/j.jtbi.2008.12.018

19. Gigante G, Deco G, Marom S, Giudice PD. Network Events on Multiple Space and Time Scales in Cultured Neural Networks and in a Stochastic Rate Model. *PLOS Computational Biology*. 2015;11(11):e1004547. doi:10.1371/journal.pcbi.1004547

20. Farokhniaee A, Lowery MM. Cortical network effects of subthalamic deep brain stimulation in a thalamo-cortical microcircuit model. *J Neural Eng*. 2021;18(5). doi:10.1088/1741-2552/abee50

21. Yousif N, Bain PG, Nandi D, Borisyuk R. A Population Model of Deep Brain Stimulation in Movement Disorders From Circuits to Cells. *Front Hum Neurosci*. 2020;14. doi:10.3389/fnhum.2020.00055

22. Wilson HR, Cowan JD. Excitatory and Inhibitory Interactions in Localized Populations of Model Neurons. *Biophysical Journal*. 1972;12(1):1-24. doi:10.1016/S0006-3495(72)86068-5

23. Tsodyks M, Wu S. Short-term synaptic plasticity. *Scholarpedia*. 2013;8(10):3153. doi:10.4249/scholarpedia.3153

24. Ghanbari A, Malyshev A, Volgushev M, Stevenson IH. Estimating short-term synaptic plasticity from pre-and postsynaptic spiking. *PLoS computational biology*. 2017;13(9):e1005738.

25. Sporns O, Chialvo DR, Kaiser M, Hilgetag CC. Organization, development and function of complex brain networks. *Trends in Cognitive Sciences*. 2004;8(9):418-425. doi:10.1016/j.tics.2004.07.008

26. Tsodyks M, Pawelzik K, Markram H. Neural networks with dynamic synapses. *Neural Comput*. 1998;10(4):821-835. doi:10.1162/089976698300017502

27. Nelder JA, Mead R. A Simplex Method for Function Minimization. *ComputJ*. 1965;7:308-313. doi:10.1093/comjnl/7.4.308

28. Lagarias JC, Reeds JA, Wright MH, Wright PE. Convergence Properties of the Nelder--Mead Simplex Method in Low Dimensions. *SIAM J Optim*. 1998;9(1):112-147. doi:10.1137/S1052623496303470

29. Shimazaki H, Shinomoto S. A method for selecting the bin size of a time histogram. *Neural Comput*. 2007;19(6):1503-1527. doi:10.1162/neco.2007.19.6.1503

30. Shimazaki H, Shinomoto S. Kernel bandwidth optimization in spike rate estimation. *J Comput Neurosci*. 2010;29(1):171-182. doi:10.1007/s10827-009-0180-4

31. Milosevic L, Kalia SK, Hodaie M, Lozano AM, Popovic MR, Hutchison WD. Physiological mechanisms of thalamic ventral intermediate nucleus stimulation for tremor suppression. *Brain*. 2018;141(7):2142-2155.

32. Pirini M, Rocchi L, Sensi M, Chiari L. A computational modelling approach to investigate different targets in deep brain stimulation for Parkinson's disease. *J Comput Neurosci*. 2008;26(1):91. doi:10.1007/s10827-008-0100-z

33. Steiner LA, Kühn AA, Geiger JR, et al. *Persistent Synaptic Inhibition of the Subthalamic Nucleus by High Frequency Stimulation*.; 2021:2021.10.20.465131. doi:10.1101/2021.10.20.465131

34. Molnar GF, Pilliar A, Lozano AM, Dostrovsky JO. Differences in neuronal firing rates in pallidal and cerebellar receiving areas of thalamus in patients with Parkinson's disease, essential tremor, and pain. *J Neurophysiol*. 2005;93(6):3094-3101. doi:10.1152/jn.00881.2004

35. Remple MS, Bradenham CH, Kao CC, Charles PD, Neimat JS, Konrad PE. Subthalamic Nucleus Neuronal Firing Rate Increases with Parkinson's Disease Progression. *Mov Disord*. 2011;26(9):1657-1662. doi:10.1002/mds.23708

36. Ramdhani RA, Patel A, Swope D, Kopell BH. Early Use of 60 Hz Frequency Subthalamic Stimulation in Parkinson's Disease: A Case Series and Review. *Neuromodulation: Technology at the Neural Interface*. 2015;18(8):664-669. doi:10.1111/ner.12288

37. Karl JA, Ouyang B, Verhagen Metman L. A Novel Dual-Frequency Deep Brain Stimulation Paradigm for Parkinson's Disease. *Neurol Ther*. 2019;8(2):483-489. doi:10.1007/s40120-019-0140-5

38. Koeglsperger T, Palleis C, Hell F, Mehrkens JH, Bötzel K. Deep Brain Stimulation Programming for Movement Disorders: Current Concepts and Evidence-Based Strategies. *Front Neurol*. 2019;10. doi:10.3389/fneur.2019.00410

39. Merola A, Zibetti M, Artusi CA, et al. 80 Hz versus 130 Hz subthalamic nucleus deep brain stimulation: effects on involuntary movements. *Parkinsonism Relat Disord*. 2013;19(4):453-456. doi:10.1016/j.parkreldis.2013.01.006

40. Valldeoriola F, Muñoz E, Rumià J, et al. Simultaneous low-frequency deep brain stimulation of the substantia nigra pars reticulata and high-frequency stimulation of the subthalamic nucleus to treat levodopa unresponsive freezing of gait in Parkinson's disease: A pilot study. *Parkinsonism Relat Disord*. 2019;60:153-157. doi:10.1016/j.parkreldis.2018.09.008

41. Anderson JS, Lampl I, Gillespie DC, Ferster D. The contribution of noise to contrast invariance of orientation tuning in cat visual cortex. *Science*. 2000;290(5498):1968-1972. doi:10.1126/science.290.5498.1968

42. Rauch A, La Camera G, Luscher HR, Senn W, Fusi S. Neocortical pyramidal cells respond as integrate-and-fire neurons to in vivo-like input currents. *J Neurophysiol*. 2003;90(3):1598-1612. doi:10.1152/jn.00293.2003

43. Lim S, McKee JL, Woloszyn L, et al. Inferring learning rules from distributions of firing rates in cortical neurons. *Nature Neuroscience*. 2015;18(12):1804-1810. doi:10.1038/nn.4158

44. Izhikevich EM, Edelman GM. Large-scale model of mammalian thalamocortical systems. *PNAS*. 2008;105(9):3593-3598. doi:10.1073/pnas.0712231105

45. Schwalger T, Chizhov AV. Mind the last spike — firing rate models for mesoscopic populations of spiking neurons. *Current Opinion in Neurobiology*. 2019;58:155-166. doi:10.1016/j.conb.2019.08.003

46. Murphy BK, Miller KD. Balanced amplification: a new mechanism of selective amplification of neural activity patterns. *Neuron*. 2009;61(4):635-648. doi:10.1016/j.neuron.2009.02.005

47. Reis C, Sharott A, Magill PJ, et al. Thalamocortical dynamics underlying spontaneous transitions in beta power in Parkinsonism. *Neuroimage*. 2019;193:103-114. doi:10.1016/j.neuroimage.2019.03.009

48. Huang CH, Lin CCK. A novel density-based neural mass model for simulating neuronal network dynamics with conductance-based synapses and membrane current adaptation. *Neural Networks*. 2021;143:183-197. doi:10.1016/j.neunet.2021.06.009

49. Girard B, Lienard J, Gutierrez CE, Delord B, Doya K. A biologically constrained spiking neural network model of the primate basal ganglia with overlapping pathways exhibits action selection. *European Journal of Neuroscience*. 2021;53(7):2254-2277. doi:10.1111/ejn.14869

50. Murray Sherman S, Guillery RW. Chapter II - The Nerve Cells of the Thalamus. In: Murray Sherman S, Guillery RW, eds. *Exploring the Thalamus*. Academic Press; 2001:19-58. doi:10.1016/B978-012305460-9/50016-2

51. Ohara PT, Chazal G, Ralston HJ. Ultrastructural analysis of gaba-immunoreactive elements in the monkey thalamic ventrobasal complex. *Journal of Comparative Neurology*. 1989;283(4):541-558. doi:10.1002/cne.902830408

52. Fleming JE, Dunn E, Lowery MM. Simulation of Closed-Loop Deep Brain Stimulation Control Schemes for Suppression of Pathological Beta Oscillations in Parkinson's Disease. *Frontiers in Neuroscience*. 2020;14:166. doi:10.3389/fnins.2020.00166

53. Mallet N, Pogosyan A, Márton LF, Bolam JP, Brown P, Magill PJ. Parkinsonian Beta Oscillations in the External Globus Pallidus and Their Relationship with Subthalamic Nucleus Activity. *J Neurosci*. 2008;28(52):14245-14258. doi:10.1523/JNEUROSCI.4199-08.2008

54. Kovaleski RF, Callahan JW, Chazalon M, Wokosin DL, Baufreton J, Bevan MD. Dysregulation of external globus pallidus-subthalamic nucleus network dynamics in parkinsonian mice during cortical slow-wave activity and activation. *J Physiol*. 2020;598(10):1897-1927. doi:10.1113/JP279232

55. Steiner LA, Tomás FJB, Planert H, Alle H, Vida I, Geiger JRP. Connectivity and Dynamics Underlying Synaptic Control of the Subthalamic Nucleus. *J Neurosci*. 2019;39(13):2470-2481. doi:10.1523/JNEUROSCI.1642-18.2019

56. Grado LL, Johnson MD, Netoff TI. Bayesian adaptive dual control of deep brain stimulation in a computational model of Parkinson's disease. *PLOS Computational Biology*. 2018;14(12):e1006606. doi:10.1371/journal.pcbi.1006606

57. Destexhe A, Rudolph M, Fellous JM, Sejnowski TJ. Fluctuating synaptic conductances recreate in vivo-like activity in neocortical neurons. *Neuroscience*. 2001;107(1):13-24. doi:10.1016/S0306-4522(01)00344-X

58. Cleary DR, Raslan AM, Rubin JE, et al. Deep brain stimulation entrains local neuronal firing in human globus pallidus internus. *J Neurophysiol*. 2013;109(4):978-987. doi:10.1152/jn.00420.2012